communications physics

Article

https://doi.org/10.1038/s42005-024-01609-6

# Enhanced sensitivity with nonlinearity-induced exceptional points degeneracy lifting

Check for updates

Haichuan Li[1,2], Lei Chen[1,2] ✉, Wenhao Wu[1,2], Hongteng Wang[1,2], Tianqi Wang[1,2], Yu Zhong[1,2], Feifan Huang[1,2], Gui-Shi Liu[1,2] ✉, Yaofei Chen[1,2], Yunhan Luo[1,2] ✉ & Zhe Chen[1,2]

Bifurcation of exceptional points (EPs), particularly higher-order EPs, can offer applications in metrology by amplifying sensitivity, but this method suffers from a tradeoff between sensitivity and robustness. To break this constraint, we experimentally introduce nonlinearity into the EP degeneracy lifting at the coupled electric resonators and observe a sixth-order nonlinear bifurcation which amplifies the sensitivity elevenfold compared to the conventional EP-based approach operating in the linear regime, while maintaining the degrees of freedom, thereby without cost in robustness. Moreover, we discover a chaotic dynamics near the EP due to the nonlinear contribution, which constitutes a distinct difference from the EP degeneracy lifting in the linear regime with random noise. Our study expands the scope of EP degeneracy lifting into nonlinearity, providing a paradigm to exploit the benefit of EPs.

Non-Hermitian degeneracy, known as exceptional points (EPs), has recently gained much attention because skewed vector space may increase symmetry by losing dimensionality[1,2]. Thus, breaking this symmetry may change the eigenfrequencies sharply, rendering a sensitive feature to external perturbations ε. The initial rationale for using EPs for sense is that the eigenfrequency splitting $\delta\omega$ of coupled elements at $N$th-order EPs scales as $\delta\omega \propto \varepsilon^{1/N}$, in contrast to linear scaling $\delta\omega \propto \varepsilon$ with diabolic points of Hermitian degeneracies[3–5]. However, such EP-enhanced sensitivity is available at a price of stringent requirements to fabrication errors[6] or advanced fine-tune technology[7,8]. Motivated by engineering a robust EP, a new notion, exceptional surface, was proposed recently[9]. Nevertheless, the exceptional surface may provide less help in $EP_N$ with a higher sensitivity for $N > 2$[10,11], remaining an open question regarding the tradeoff between sensitivity and robustness.

In essence, addressing this tradeoff is challenging in the linear regime. The reason is attributed to the sensitivity of a linear system depending on its degeneracy. Specifically, a higher sensitivity must possess more degrees of freedom to maintain degeneracy, reducing a system's robustness[4,11,12]; otherwise, a higher-order EP would split into several lower-order EPs, decreasing sensitivity[13]. Fortunately, the rapidly developed optical microcavity allows us to access nonlinear regimes by capturing light power within a tiny size[14–17], and as a result, a pioneering theoretical report regarding optical parametric oscillators in resonators has generated four branches from $EP_2$ degeneracy lifting, which offers an avenue to enhance sensitivity using fewer degrees of freedom[18]. However, such favorite nonlinearity-induced EP degeneracy lifting is difficult to observe in optics because of the sensitive phase matching condition and microcavity detune[19,20]. More recently, the trait of $EP_2$ above the laser threshold predicted such multi-branches degeneracy lifting, but the experiments failed to observe[21].

Due to the homeomorphism of the wave equation and Schrödinger equation, electrical microcavity has gradually developed as an essential platform for studying EP-based physics[22]. Compared to coupled optical counterparts, it possesses unique advantages like compact size and noise suppression. For example, a negative resistance circuit can serve as a gain directly without requiring an extra wavelength pump in optics, providing a compact size[23–25]. Besides, after a proper lowpass design, the electrical microcavity may reduce the thermal noise around a higher-order EP comparable to a diabolic point in the Hermitian situation[26]. More importantly, electrical microcavity can couple modes with a detuned frequency, offering an alternative protocol, *anti-PT* symmetry[27], to harness EPs. In addition, the electrical system easily yields the nonlinear effect[28]. For example, the diode provides voltage-dependent resistor value, generating $EP_3$ in two coupled electrical resonators[29]. However, most contributions

[1]Department of Optoelectronic Engineering, College of Physics and Optical Engineering, Jinan University, Guangzhou 510632, China. [2]Guangdong Provincial Key Laboratory of Optical Fiber Sensing and Communications; Key Laboratory of Optoelectronic Information and Sensing Technologies of Guangdong Higher Education Institutes, Jinan University, Guangzhou 510632, China. ✉e-mail: chenlei@jnu.edu.cn; guishiliu@163.com; yunhanluo@163.com

have focused on the intensity-induced nonlinear effects akin to the Kerr effect in nonlinear optics[28–30].

This study experimentally showcases a nonlinear phenomenon, multi-branch EP degeneracy lifting, using *anti-PT* electrical resonators, similar to the four-wave mixing in nonlinear optics. The study found that nonlinear interaction among eigenmodes under the *anti-PT* symmetric-breaking phase yields up to twelfth-order $EP_2$ degeneracy lifting. In terms of identical limit of detection, a sixth-order nonlinear bifurcation amplifies the sensitivity by elevenfold compared to the conventional EP-based sensing operating in the linear regime. Unlike previous explorations of EPs in the linear regime, the nonlinearity-induced EP degeneration lifting produces a chaotic dynamic instead of random noise. This sensing protocol enhances sensitivity by over one order of magnitude and expands the scope of bifurcation into nonlinearity, providing a paradigm to exploit the benefits of EPs.

## Results

### Sensing scheme

To understand the role of the nonlinear effect in the EP degeneracy lifting, we compared three types of bifurcations on the $EP_2$, $EP_3$, and $EP_2$ with nonlinearity involvement in Fig. 1. Figure 1a, b exhibit the sinusoidal waves dynamics of the most common situation of $EP_2$ and $EP_3$. From their spectra obtained by Fourier transformation, we find that after bifurcation their eigenfrequencies are composed of two or three branches in Fig. 1d, e, identical to their $EP_N$'s degrees of freedom. In contrast, when the dynamics of the eigenmodes hold a non-sinusoidal fashion in Fig. 1c, its eigenfrequencies after bifurcation engender nonlinear components in Fig. 1f, producing more branches far beyond $EP_N$'s degrees of freedom, and the extended gaps between each branch pair may merit higher sensitivity for sensing application.

### Circuits with nonlinearity-induced EP degeneracy lifting

To experimentally demonstrate this non-linearity in bifurcation, we have fabricated an *anti-PT* electric circuit with an engineered EP, as shown in Fig. 2a. The *anti-PT* electric circuit includes two LRC resonators, coupling by a resistor $R_c$. Each resonator is composed of a negative resistor unit $-\widetilde{R}_j$, a capacitor $C_j$, and an inductor $L_j$, where $j$ denotes resonator indexes. Applying Kirchhoff's circuit laws, the circuit diagram can be simplified as

$$V_1 - V_2 = R_C I_C + P^{NL} \tag{1}$$

$$V_j = -L_j \frac{dI_{Lj}}{dt} = -\frac{1}{C_j}\int_0^t I_{Cj}(\tau)d\tau = R_j I_{Rj} \tag{2}$$

$$I_C = I_{L1} + I_{C1} + I_{R1} = -(I_{L2} + I_{C2} + I_{R2}) \tag{3}$$

where $I_{Lj}$, $I_{Cj}$, and $I_{Rj}$ are electrical currents at $L_j$, $C_j$, and $-R_j$, respectively; $P^{NL}$ is the nonlinear component, contributed by $-R_j$. With the ansatz of $V_j = v_j(t)e^{-i\omega_0 t}$, we achieve the coupled differential equations

$$\frac{d}{dt}\begin{pmatrix} v_1 \\ v_2 \end{pmatrix} = \underbrace{\frac{1}{\eta - 2i}\begin{bmatrix} -\Delta & -i\alpha/2 \\ -i\alpha/2 & \Delta \end{bmatrix}\begin{pmatrix} v_1 \\ v_2 \end{pmatrix}}_{Linear} + \underbrace{\frac{i\alpha}{2\omega_0}P^{NL}e^{i\omega_0 t}}_{Nonlinear} \tag{4}$$

where $\eta = \beta/\omega_0$ and $\Delta = (\omega_2 - \omega_1)/2$, with the note of $\omega_j = (L_j C)^{-1/2}$, $\omega_0 = (\omega_1 + \omega_2)/2$, $\alpha = (R_c C)^{-1}$, and $\beta = C^{-1}(R_C^{-1} - R_j^{-1})$ in terms of $C_j = C$. Note that the linear component dominates if $R_c = R$, yielding $\eta = 0$[27]; in contrast, we set $R_c > R$ to stimulate the nonlinear components in the negative resistor (see methods). The solution achieved from the linear components should be $v(t) = v_+ e^{-i\omega_+ t} + v_- e^{-i\omega_- t} + c.c.$, where $\omega_\pm = \pm\sqrt{\alpha^2/4 - \Delta^2} = \pm\delta$ are the eigenfrequencies. As a result, the nonlinear components can be expressed as

$$P^{NL}(t) = \sum_k \int \chi^{(k)}(t-\tau)v^k(\tau)d\tau \tag{5}$$

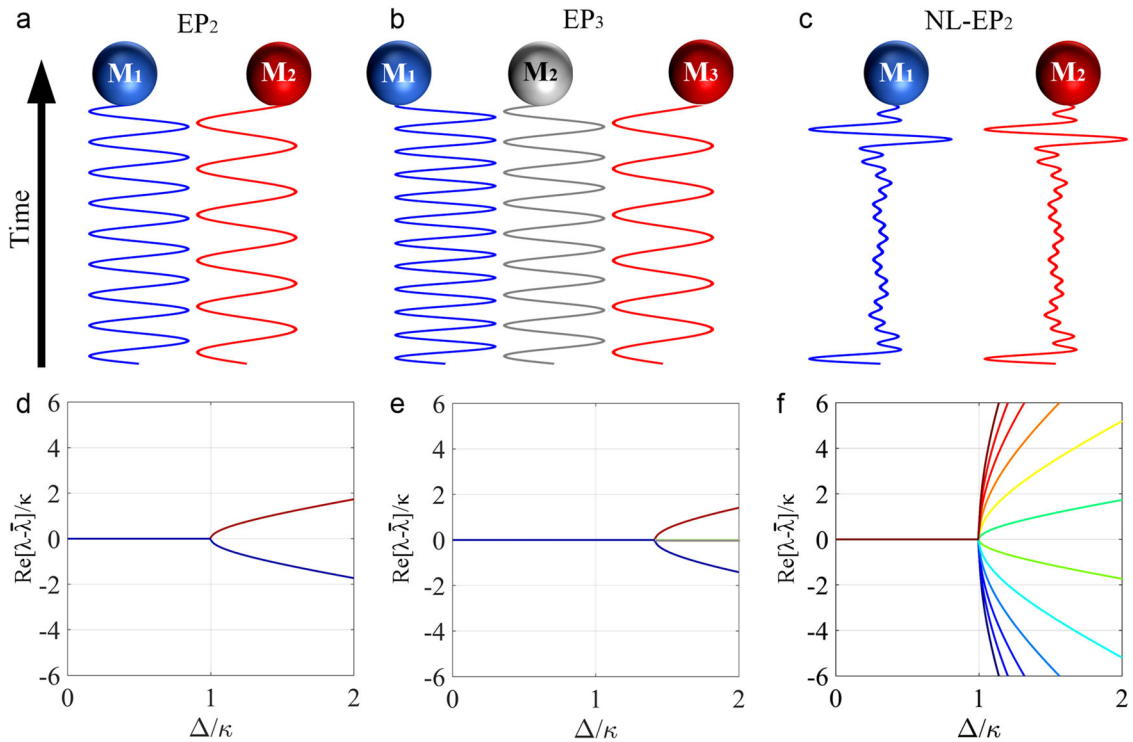


**Fig. 1 | Schematic of eigenmode dynamics and corresponding eigenfrequencies real parts.** Dynamics of **a** $EP_2$, **b** $EP_3$, and **c** $EP_2$ with nonlinearity, where EP stands for exceptional point. $M_1$, $M_2$, and $M_3$ are eigenmodes supported by a coupled system. Real parts of system eigenfrequencies $\lambda$ of **d** $EP_2$, **e** $EP_3$, and **f** $EP_2$ with nonlinearity, where $\bar{\lambda}$ is the mean value of eigenvalues; $\Delta$ and $\kappa$ are the detuning and coupling strength. The color of solid curves represents the value of $\mathrm{Re}[\lambda\text{-}\bar{\lambda}]/\kappa$, with red indicating a higher value and blue indicating a lower value.

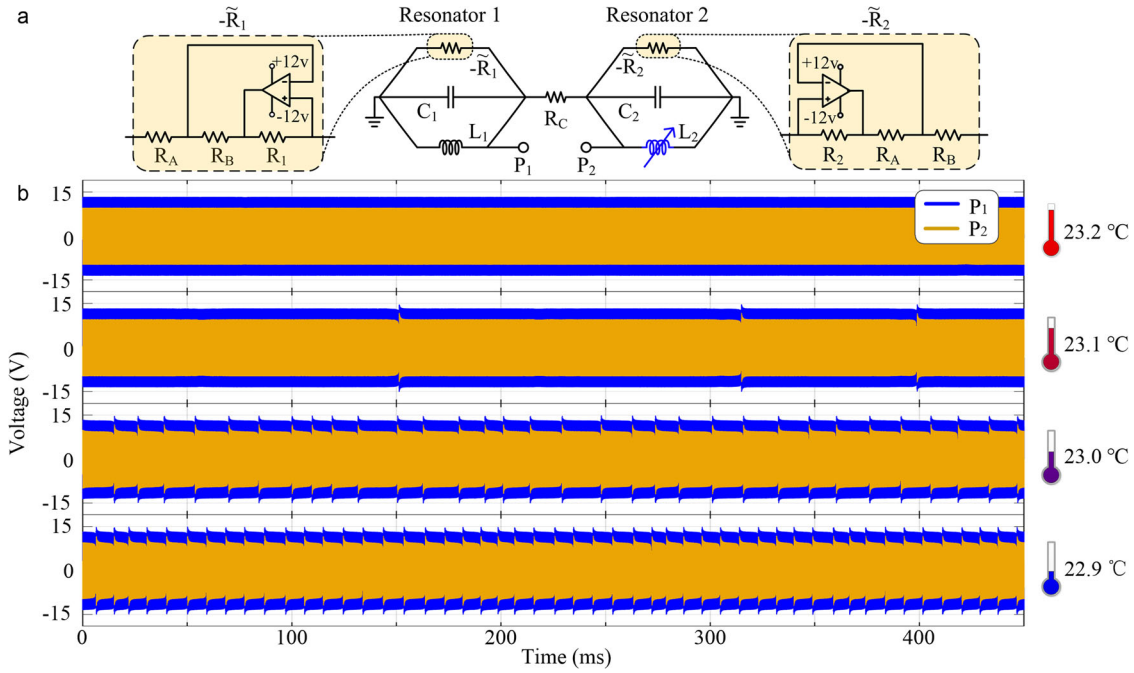


**Fig. 2 | *Anti-PT* electric resonators and their response in the time domain. a** The *anti-PT* circuit diagram, where R, C, L are the resistor, capacitor, and inductor; **b** Voltage dynamics of probes $P_1$ and $P_2$ at temperatures of 23.2, 23.1, 23.0, and 22.9 °C.

where $\chi^{(k)}$ is the equivalent nonlinear susceptibility, and $k \in Z$ is the nonlinear order. Thus, $v_{sum}(t)$ including linear and nonlinear components can be spanned by $v_{sum}(t) = \sum_k v_k \cos k\delta t$, generating sharp changes in the time domain. Such a result is similar to the four-wave mixing in nonlinear optics, creating terms of $(2\omega_+ - \omega_-) + k(\omega_+ - \omega_-)$ with an extended gap between a branch pair from $2\delta$ to $2(2k\text{-}1)\delta$. Note that linear components yield these nonlinear eigenfrequencies, thereby resulting in an inherent degeneracy. The degrees of freedom are identical to the $EP_2$-based protocol, and thus, the increased sensitivity is no cost in robustness like high-order EP sensors.

To stimulate the nonlinear components, we selected the parameters of $R_C = 400\ \Omega$, $R_1 = R_2 = 100\ \Omega$, $C = 225$ nF, $L_1 = 1.441$ mH. Motivated by controlling $\Delta$ through $\omega_2$, a lab-made temperature controller with a resolution of 0.01 °C was deployed, adjusting the temperature of $L_2$, and the measured value of $L_2$ at ~1 mH is linearly dependent on temperature with a sensitivity of ~0.5 μH/°C. Later, we observe the circuit's *anti-PT* phase transition by monitoring $P_1$ and $P_2$ in Fig. 2a. When the temperature of $L_2$ was kept at 23.2 °C, the system entered an anti-PT symmetric phase. In contrast to the theoretically expected amplifying envelope, both probes remained flat due to the limited power supply. Later, several sharply changed peaks appeared in their envelopes if we cooled down the temperature to 23.1 °C, demonstrating the expected nonlinearity in Eq. (5). These peaks emerged in an aperiodic fashion when the system approached EP. After that, the system accessed the *anti-PT* symmetric-breaking phase when the temperature was reduced to 23.0 °C. The aperiodic peaks in the envelope nearly disappeared if we further decreased the temperature to 22.9 °C.

Motivated by observing the nonlinearity-induced EP degeneracy lifting, we have carried out a more accurate temperature control with a step of 0.05 °C and implemented Fourier transformation on $P_1$ and $P_2$, as shown in Fig. 3a, b. The *anti-PT* symmetric-breaking phase emerges multiple branches due to the contribution from nonlinearity when the temperature is below 23.1 °C, and the available nonlinear order is even up to twelve. Compared to Fig. 3a, b, the spectra vary with the temperature of $L_2$, presenting a phase transition in the vicinity of 23.1 °C independent of orders, and the nearly identical evolution reveals the energy-difference conservation and synchronized power oscillation in the *anti-PT* symmetric phase[31].

We can note that the background spectra for the *anti-PT* symmetric-breaking phase increases, compared to the *anti-PT* symmetric phase. In general, the *anti-PT* symmetric-breaking phase generates the oscillated dynamics with increasing intensity, but the practical power cannot sustain the infinite value. As a result, the dynamics yield a sine oscillation, generating a single peak in the spectra with weak background spectra. In contrast, when the *anti-PT* symmetric phase dynamics evolve complicated due to the nonlinear contribution, the dynamics possess uneven peaks, causing a slight background spectra of <−25 dB.

To quantify the background components, we have analyzed the Allan deviation of $P_1$ versus the time of neighboring peaks near the EP, as shown in Fig. 3c. At a temperature of 23.2 °C, $\sigma(\tau)$ is highly weak $<\sim 10^{-7}$, indicating the presence of a weak background. The decreased $\sigma(\tau)$ with a function between $\tau^{-1/2}$ and $\tau^{-1}$ demonstrates the coexistence of the quantization noise and white noise in the *anti-PT* symmetric-breaking phase. The white noise in $P_1$ results from thermal noise from the circuit elements[30], but the quantization noise comes from our treatment in math rather than sampling time because we employed the time gap between two neighboring peaks to consider nonlinear spectra components. As T decreased to 23.1 °C, the system approaches EP, where $\sigma(\tau)$ increased dramatically $\sim 10^3$, and $\sigma(\tau)$ approaches $\tau^{-1/2}$, indicating white noise, that is, thermal noise, becomes dominant. The white noise plays the leading role in the short-time readout when T further drops to 23.0 °C. However, its impact vanished for a longer readout, and bias insatiability appears at $\tau \sim 10^4$, which stems from the random flickering of electronics or other system components. For T = 22.9 °C, the *anti-PT* symmetric phase disappears the bias insatiability, leading to a reduced $\sigma(\tau)$ and verifying the reduced signal noise ratio on EP.

## Chaotic dynamics feature

Another interesting and significant characteristic of EP is the fluctuation near EP[32,33]. In general, EPs may cause random noise[34] due to the dissipative essence under the linear theoretical frame according to the theory of quantum Fisher information[35]. In parallel to the progress of randomness around EP, chaotic dynamics are ubiquitously in various practical physical settings under nonlinear regimes[36,37]. Thus, two natural questions arose for the nonlinearity-induced degeneracy lifting: (I) Do the fluctuations occur around EP? (II) Is it chaotic or random?

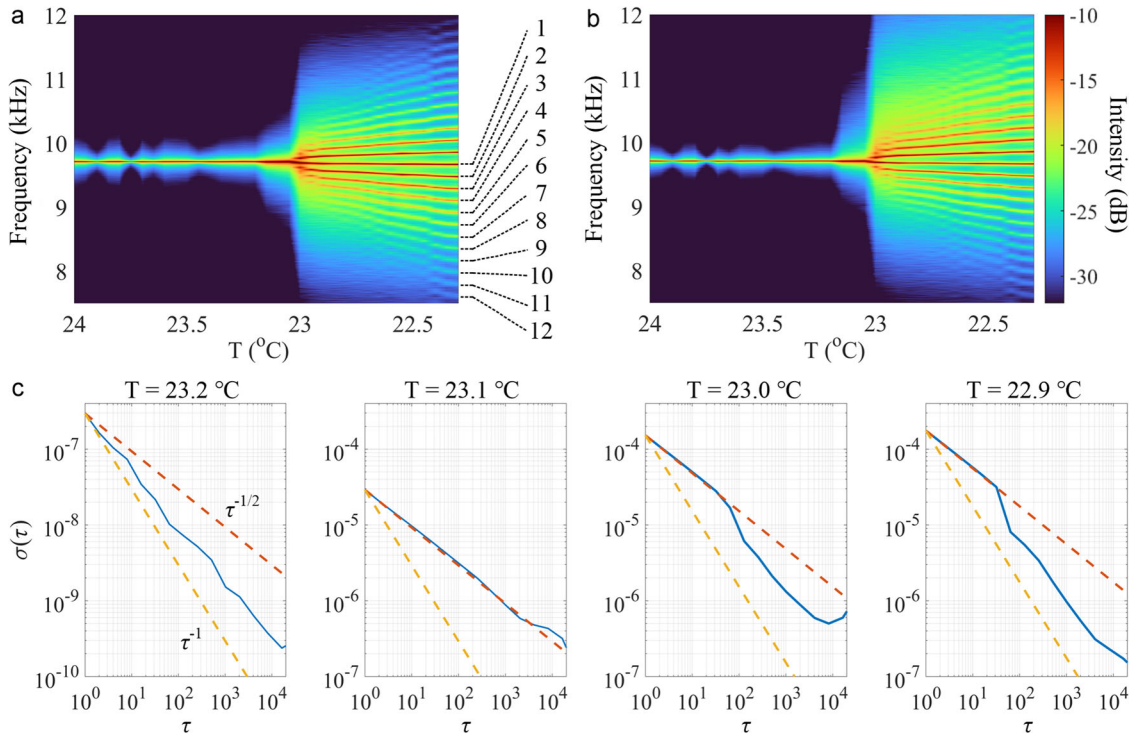


**Fig. 3 | Changes in the spectra with the temperature of the inductor $L_2$.** Spectra versus temperature at probes **a** $P_1$ and **b** $P_2$, where multiple branches emerge at the anti-PT symmetric-breaking phase. The numbers describe the order of nonlinearity degeneracy, and their counterpart at the blueshift are not labeled. **c** Allan deviation $\sigma(\tau)$ of $P_1$ shown in blue curves versus the time of each neighboring peak $\tau$ at different temperatures, where dashed lines in red and orange are $\tau^{-1/2}$ and $\tau^{-1}$.

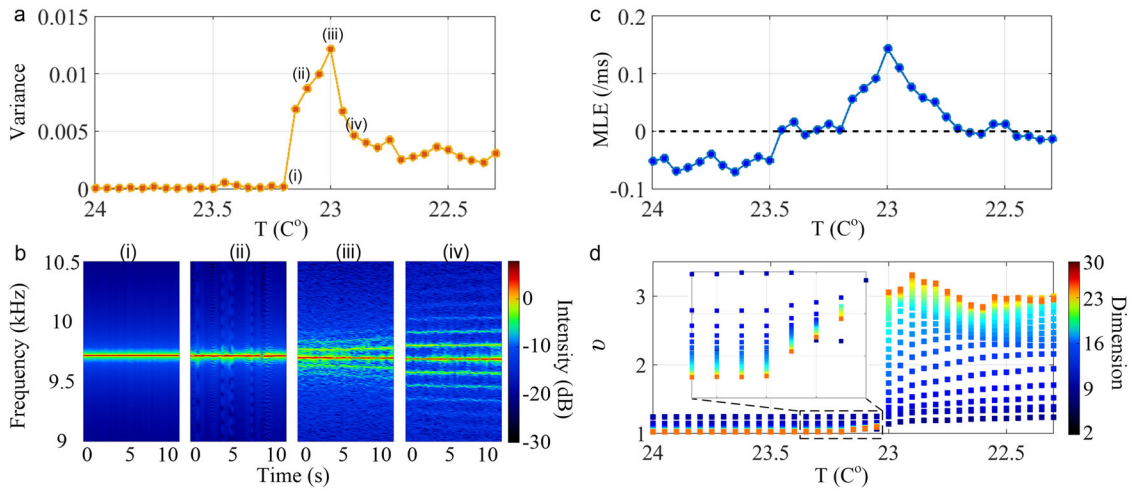


**Fig. 4 | Chaotic characteristic analysis. a** Variance of the spectra as a function of temperature; **b** Examples of time evolution of the spectra in **a**; **c** dependence of maximum Lyapunov exponent (MLE) on the temperature; **d** dependence of the correlation dimension (υ) on the temperature. The dimension in the calculation is taken from 2 to 30, marked by color from blue to red. The dots present a convergence behavior towards increasing dimensions at each temperature, confirming a non-random character.

For the first question, we have observed an aperiodic peak in the envelope near EP at ~23.1 °C in Fig. 2b. To quantify such fluctuations, we calculated the variance of spectra within 10 s in the step of 0.5 s, as shown in Fig. 4a, and we provided four typical spectral variances in Fig. 4b to aid visualization. The spectra variance in the *anti-PT* symmetric phase is nearly constant where the temperature of $L_2$ is higher than 23.2 °C. By contrast, a sharp change appears when its temperature is slightly cooled to 23.15 °C, corresponding to an EP. A further decreased temperature generates a more extended spectra variance, and later, the spectra variance drops quickly to ~0.003.

For the second question, we have calculated the most commonly used maximum Lyapunov index (MLE) in Fig. 4c. In general, a positive MLE indicates chaotic behavior, and experiments show that its MLE is above zero if the temperature closes EP[38,39]. Likewise, the correlation dimension ($\upsilon$) is another landmark in estimating chaotic behavior, and a time series is chaotic if $\upsilon$ takes a non-integer[40]. Figure 4d displays that $\upsilon$ leaves integer one and takes non-integer when the temperature is slightly below 23.2 °C. A further reduction in temperature produces a transition, but $\upsilon$ maintains a non-integer if the temperature is above 22.55 °C, consistent with the chaotic estimation from MLE. Except for the region in the vicinity of EP, $\upsilon$

approaches integers one and three when the temperature is below 22.55 °C and above 23.2 °C. Generally, $\upsilon = 1$ indicates sinusoidal dynamics, accounting for the oscillation in the *anti-PT* symmetric phase, and $\upsilon = 3$ suggests more complex periodic dynamics, such as periodic oscillation with a rapidly changed envelope in the *anti-PT* symmetric-breaking phase.

Such chaotic behavior may bring a sensing protocol in utilizing EP for pursuing accuracy because chaos, in principle, is deterministic instead of random[41,42]. For example, reservoir computing has been used to forecast the time series with Lyapunov time ~10 [43–45], and the continued rapid pace of improvement in computing performance may forecast a longer Lyapunov time. Thus, their combination would facilitate multidisciplinary cooperation among artificial intelligence, chaos, and sensing for the foreseeable future.

### Results of enhanced sensitivity

To examine the nonlinear degeneracy lifting, we define the sensitivities of corresponding nonlinear order $k$ by $S \equiv \partial(2k\delta)/\partial T$, where T is temperature, and plot the sensitivity depending on the temperature under different orders in Fig. 5a. The Puiseux series is a helpful tool for performing complex analysis around an EP, and several elegant reports have presented the bifurcation for an $EP_2 \propto \varepsilon^{1/2}$ [8,24]. A log-log scale of the sensitivity to temperature in Fig. 5a may better visualize the theory, where the bottom curve describes the first-order degeneracy lifting of $EP_2$, and the others depict that of higher-order. The responses are linearly dependent on the temperature perturbation, and the slopes of all curves in Fig. 5b approach 1/2 independently of the orders because higher-order nonlinearity is attributed to the first-order components, experimentally verifying the nonlinearity-induced degeneracy lifting.

Such a degeneracy lifting mechanism merits a superior performance in sensing because of a more extended gap in spectra. To quantify the benefit of nonlinearity, we define an enhancement factor, that is, the ratio of the higher-order sensitivity and first-order sensitivity, and Fig. 5c shows that the enhancement factor is proportional to the order of nonlinearity, which is consistent with Eq. (5). In terms of the unchanged limit of detection, a sixth-

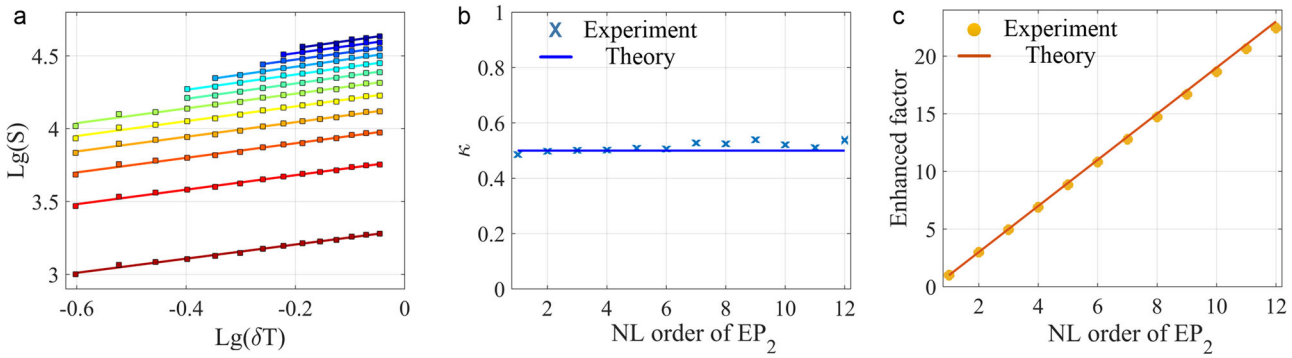


**Fig. 5 | Results of enhanced sensitivity. a** The log-log scale of sensitivity depends on the perturbation in temperature at probe $P_1$. Squares and curves are the experiments and fitting results, where the nonlinear order increases from 1 to 12 from bottom to up. The beginning temperature is 22.95 °C, where spectra have a negligible impact from chaos. Here, we do not show the sensitivity of probe $P_2$ because of the resembling result; **b** Slops, and **c** enhanced factor of various nonlinear (NL) orders.

**Fig. 6 | Four-wave mixing-like nonlinearity stimulation. a** Dynamics of probe $P_1$ with various coupling resistor $R_c$ from 100 Ω to 500 Ω. **b** corresponding spectra of Fig. 6a.

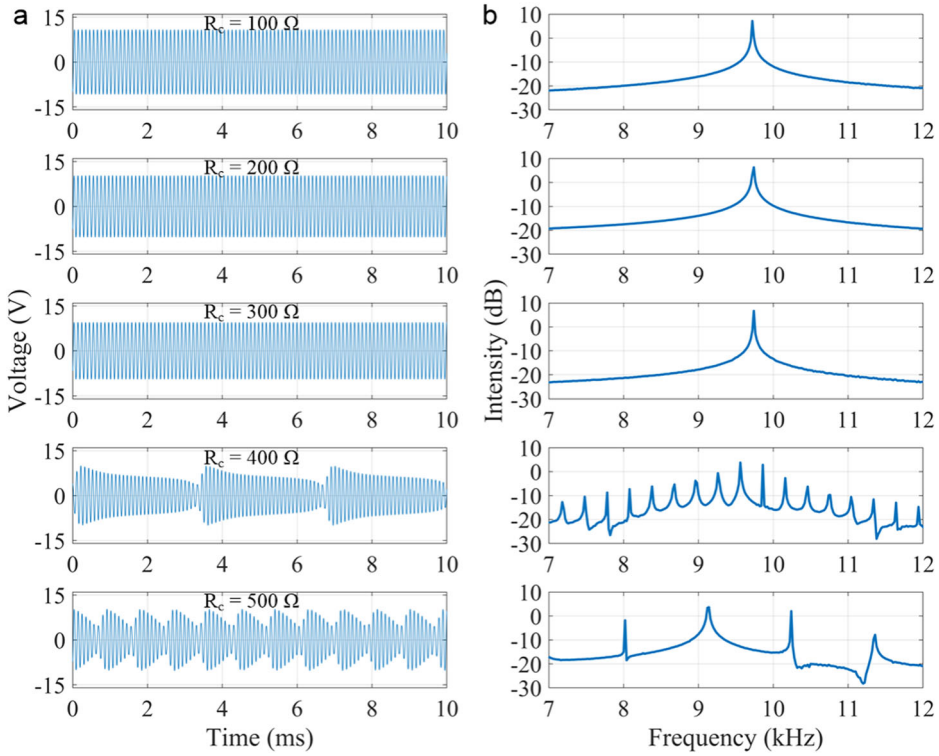

order nonlinear bifurcation amplifies sensitivity by eleven folds than that of the conventional $EP_2$ scenario in the linear regime. Except for the advantageous near EP, such a nonlinear signature compensates for the drawback of the EP-based method operating in the linear regime in a reduced sensing range. Specifically, the sensing strategy with the fashion of $\varepsilon^{1/N}$ must sacrifice the sensitivity for $\varepsilon > 1$ situation. However, for the nonlinearity-induced protocol, a greater enhancement is achieved for the higher order without losing the performance in larger perturbation, offering an extended sensing range.

## Conclusions

In summary, this letter observed the nonlinear-induced EP degeneracy lifting at the electric resonators, where a bifurcation yields up to twenty-four branches, corresponding to twelfth-order nonlinearity. In terms of the unchanged limit of detection, a sixth-order nonlinear bifurcation amplifies the sensitivity eleven-fold compared to the conventional $EP_2$-based sensing in the linear regime. Still, the degrees of freedom for the nonlinear bifurcation are identical to that of the $EP_2$-based sensing protocol, thereby endowing a robust performance and breaking the constrict between sensitivity and robustness. Moreover, such nonlinearity-induced EP degeneracy lifting amplifies the sensitivity independent of the sensing range, compensating for the disadvantage of the EP-based method operating in the linear regime for $\varepsilon > 1$ situation. More interestingly, we discovered the determined chaotic dynamics near EPs due to the nonlinear contribution, which presents a distinct difference from the random noise character in the linear regime. This letter expands the scope of EP degeneracy lifting into nonlinearity and enhances the sensitivity beyond one order of magnitude. More importantly, our study bridges chaotic dynamics and bifurcation, providing a paradigm to exploit the benefit of EPs.

## Methods

### Experimental measurements

The *anti-PT* circuit diagram consists of two coupled LRC resonators, where a dual operational amplifier chip (Maxim Integrated, MAX44248ASA+) was employed to reduce experimental errors. We used a lab-made temperature controller with an accuracy of 0.01 °C to manipulate the temperature of $L_2$. Experiments adopted the sampling rate of $2^{20}$ dots/s and 10 s/measurement to distinguish these higher-order branches in spectra.

### Nonlinearity stimulation

The four-wave mixing-like nonlinearity rises from the negative resistor, which can be stimulated when the $R_c > R$. Here, we simulated a series $R_c$ from 100 Ω to 500 Ω using *LTSpice* to demonstrate such a phenomenon. Figure 6a shows the results, and Fig. 6b displays their spectra. When $R_c = 100\ \Omega$, the linear component dominates, which has also been verified by Ref. 27. In contrast, when Rc increases to 400 Ω, such four-wave mixing-like nonlinearity is generated. In principle, a larger Rc may generate a more significant nonlinearity, but it needs a matched inductor and capacitor to achieve an EP. Considering the achievable inductors and capacitors, we employed Rc = 400 Ω in experiments.

## Data availability

All data needed to evaluate the findings of the paper are available within the paper itself. Additional data related to this paper are available from the corresponding author upon reasonable request.

## Code availability

The codes that were used for the findings of this study are openly available in the GitHub repository (https://github.com/xiiiiiiiijun/paper-code-for-Enhanced-sensitivity-with-nonlinearity-induced-exceptional-points-degeneracy-lifting).

Received: 2 February 2024; Accepted: 26 March 2024;
Published online: 05 April 2024

## References

1. El-Ganainy, R. et al. Non-Hermitian physics and PT symmetry. *Nat. Phys.* **14**, 11–19 (2018).
2. Li, T., Gao, Z. & Xia, K. Nonlinear-dissipation-induced nonreciprocal exceptional points. *Opt. Express* **29**, 17613–17627 (2021).
3. Hodaei, H. et al. Enhanced sensitivity at higher-order exceptional points. *Nature* **548**, 187–191 (2017).
4. Zhang, S. M., Zhang, X. Z., Jin, L. & Song, Z. High-order exceptional points in supersymmetric arrays. *Phys. Rev. A* **101**, 033820 (2020).
5. Wu, Y., Zhou, P., Li, T., Wan, W. & Zou, Y. High-order exceptional point based optical sensor. *Opt. Express* **29**, 6080–6091 (2021).
6. Mortensen, N. A. et al. Fluctuations and noise-limited sensing near the exceptional point of parity-time-symmetric resonator systems. *Optica* **5**, 1342–1346 (2018).
7. Wiersig, J. Enhancing the Sensitivity of Frequency and Energy Splitting Detection by Using Exceptional Points: Application to Microcavity Sensors for Single-Particle Detection. *Phys. Rev. Lett.* **112**, 203901 (2014).
8. Chen, W., Kaya, Özdemir, Ş., Zhao, G., Wiersig, J. & Yang, J. L. Exceptional points enhance sensing in an optical microcavity. *Nature* **548**, 192–196 (2017).
9. Zhong, Q. et al. Sensing with Exceptional Surfaces in Order to Combine Sensitivity with Robustness. *Phys. Rev. Lett.* **122**, 153902 (2019).
10. Qin, G. Q. et al. Experimental Realization of Sensitivity Enhancement and Suppression with Exceptional Surfaces. *Laser Photonics Rev.* **15**, 2000569 (2021).
11. Zhong, Q., Kou, J., Özdemir, Ş. K. & El-Ganainy, R. Hierarchical Construction of Higher-Order Exceptional Points. *Phys. Rev. Lett.* **125**, 203602 (2020).
12. Zhang, X.-Z., Wu, L.-T., Luo, R.-Z. & Chen, J. Higher-order exceptional points using lossfree negative-index materials. *Phys. Scr.* **98**, 095511 (2023).
13. Mandal, I. & Bergholtz, E. J. Symmetry and Higher-Order Exceptional Points. *Phys. Rev. Lett.* **127**, 186601 (2021).
14. Kippenberg, T. J., Spillane, S. M. & Vahala, K. J. Kerr-Nonlinearity Optical Parametric Oscillation in an Ultrahigh-QToroid Microcavity. *Phys. Rev. Lett.* **93**, 083904 (2004).
15. Zhang, X. et al. Symmetry-breaking-induced nonlinear optics at a microcavity surface. *Nat. Photonics* **13**, 21–24 (2018).
16. Chen, J.-H. et al. Microcavity Nonlinear Optics with an Organically Functionalized Surface. *Phys. Rev. Lett.* **123**, 173902 (2019).
17. Yang, Y.-H. et al. Nonlinear Optical Radiation of a Lithium Niobate Microcavity. *Phys. Rev. Appl.* **19**, 034087 (2023).
18. Roy, A. et al. Nondissipative non-Hermitian dynamics and exceptional points in coupled optical parametric oscillators. *Optica* **8**, 415–421 (2021).
19. Roy, A., Jahani, S., Langrock, C., Fejer, M. & Marandi, A. Spectral phase transitions in optical parametric oscillators. *Nat. Commun.* **12**, 835 (2021).
20. Jahani, S., Roy, A. & Marandi, A. Wavelength-scale optical parametric oscillators. *Optica* **8**, 262–268 (2021).
21. Ji, K. et al. Tracking exceptional points above the lasing threshold. *Nat. Commun.* **14**, 8304 (2023).
22. Assawaworrarit, S., Yu, X. & Fan, S. Robust wireless power transfer using a nonlinear parity–time-symmetric circuit. *Nature* **546**, 387–390 (2017).
23. Fernández-Alcázar, L. J., Kononchuk, R. & Kottos, T. Enhanced energy harvesting near exceptional points in systems with (pseudo-) PT-symmetry. *Commun. Phys.* **4**, 79 (2021).
24. Kononchuk, R., Cai, J., Ellis, F., Thevamaran, R. & Kottos, T. Exceptional-point-based accelerometers with enhanced signal-to-noise ratio. *Nature* **607**, 697–702 (2022).

25. Yang, M., Zhu, L., Zhong, Q., El-Ganainy, R. & Chen, P.-Y. Spectral sensitivity near exceptional points as a resource for hardware encryption. *Nat. Commun.* **14**, 1–9 (2023).
26. Xiao, Z., Li, H., Kottos, T. & Alù, A. Enhanced Sensing and Nondegraded Thermal Noise Performance Based on PT-Symmetric Electronic Circuits with a Sixth-Order Exceptional Point. *Phys. Rev. Lett.* **123**, 213901 (2019).
27. Choi, Y., Hahn, C., Yoon, J. W. & Song, S. H. Observation of an anti-PT-symmetric exceptional point and energy-difference conserving dynamics in electrical circuit resonators. *Nat. Commun.* **9**, 2182 (2018).
28. Nikzamir, A. & Capolino, F. Highly Sensitive Coupled Oscillator Based on an Exceptional Point of Degeneracy and Nonlinearity. *Phys. Rev. Appl.* **18**, 054059 (2022).
29. Bai, K. et al. Nonlinearity-enabled higher-order exceptional singularities with ultra-enhanced signal-to-noise ratio. *Natl Sci. Rev.* **10**, nwac259 (2023).
30. Suntharalingam, A., Fernandez-Alcazar, L., Kononchuk, R. & Kottos, T. Noise resilient exceptional-point voltmeters enabled by oscillation quenching phenomena. *Nat. Commun.* **14**, 5515 (2023).
31. Park, S. et al. Optical Energy-Difference Conservation in a Synthetic Anti-PT-Symmetric System. *Phys. Rev. Lett.* **127**, 083601 (2021).
32. Pick, A. et al. General theory of spontaneous emission near exceptional points. *Opt. Express* **25**, 12325–12348 (2017).
33. Duggan, R., Mann, S. A. & Alù, A. Limitations of Sensing at an Exceptional Point. *ACS Photonics* **9**, 1554–1566 (2022).
34. Zhang, M. et al. Quantum Noise Theory of Exceptional Point Amplifying Sensors. *Phys. Rev. Lett.* **123**, 180501 (2019).
35. Anderson, D., Shah, M. & Fan, L. Clarification of the Exceptional-Point Contribution to Photonic Sensing. *Phys. Rev. Appl.* **19**, 034059 (2023).
36. Huang, F. et al. Tunable anti–parity-time-symmetric chaos in optomechanics. *Phys. Rev. A* **104**, L031503 (2021).
37. Defoort, M., Rufer, L., Fesquet, L. & Basrour, S. A dynamical approach to generate chaos in a micromechanical resonator. *Microsyst. Nanoeng.* **7**, 1–11 (2021).
38. Chen, L. et al. Non-Hermitian-enhanced topological protection of chaotic dynamics in one-dimensional optomechanics lattice. *Chaos Solit. Fractals* **164**, 112678 (2022).
39. Deng, Y. et al. Mid-infrared hyperchaos of interband cascade lasers. *Light Sci. Appl.* **11**, 1–10 (2022).
40. Ma, C.-G., Xiao, J.-L., Xiao, Z.-X., Yang, Y.-D. & Huang, Y.-Z. Chaotic microlasers caused by internal mode interaction for random number generation. *Light Sci. Appl.* **11**, 1–10 (2022).
41. Gao, H. et al. 0.75 Gbit/s high-speed classical key distribution with mode-shift keying chaos synchronization of Fabry–Perot lasers. *Light Sci. Appl.* **10**, 1–9 (2021).
42. Chen, L. et al. Chaotic dynamics on exceptional surfaces. *Phys. Rev. A* **105**, L031501 (2022).
43. Pathak, J., Hunt, B., Girvan, M., Lu, Z. & Ott, E. Model-Free Prediction of Large Spatiotemporally Chaotic Systems from Data: A Reservoir Computing Approach. *Phys. Rev. Lett.* **120**, 024102 (2018).
44. Shahi, S., Fenton, F. H. & Cherry, E. M. Prediction of chaotic time series using recurrent neural networks and reservoir computing techniques: A comparative study. *Mach. Learn. Appl.* **8**, 100300 (2022).
45. Rafayelyan, M., Dong, J., Tan, Y., Krzakala, F. & Gigan, S. Large-Scale Optical Reservoir Computing for Spatiotemporal Chaotic Systems Prediction. *Phys. Rev. X* **10**, 041037 (2020).


## Acknowledgements

This work has been supported by the National Natural Science Foundation of China (61904067, 61805108, 62075088, 62175094, 62105381), Basic and Applied Basic Research Foundation of Guangdong province (2024A1515012609,2024A1515030155, 2022A1515010272, 2023A1515011459, 2022A1515011671, 2020A1515011498, 2022A1515140055), Guangdong Provincial Innovation and Entrepreneurship Training Program For Undergraduate (S202310559188), Science and Technology Projects in Guangzhou (202102020758, 202201010553).

## Author contributions

L.C. conceived the project. L.C., H.L., F.H. designed the electronic circuits. L.C., H.L., H.W., T.W., W.W. conducted the measurements. L.C. developed the theoretical framework. G.-S. L., Y.C., Z.Y., Y.L., Z.C. analyzed the data. All authors contributed to the manuscript writing.

## Competing interests

The authors declare no competing interests.

## Additional information

**Supplementary information** The online version contains supplementary material available at https://doi.org/10.1038/s42005-024-01609-6.

**Correspondence** and requests for materials should be addressed to Lei Chen, Gui-Shi Liu or Yunhan Luo.

**Peer review information** *Communications Physics* thanks the anonymous reviewers for their contribution to the peer review of this work. A peer review file is available.

**Reprints and permissions information** is available at http://www.nature.com/reprints

**Publisher's note** Springer Nature remains neutral with regard to jurisdictional claims in published maps and institutional affiliations.

**Open Access** This article is licensed under a Creative Commons Attribution 4.0 International License, which permits use, sharing, adaptation, distribution and reproduction in any medium or format, as long as you give appropriate credit to the original author(s) and the source, provide a link to the Creative Commons licence, and indicate if changes were made. The images or other third party material in this article are included in the article's Creative Commons licence, unless indicated otherwise in a credit line to the material. If material is not included in the article's Creative Commons licence and your intended use is not permitted by statutory regulation or exceeds the permitted use, you will need to obtain permission directly from the copyright holder. To view a copy of this licence, visit http://creativecommons.org/licenses/by/4.0/.

© The Author(s) 2024